# Pressure Unfolding of Proteins: New Insights Into the Role of Bound Water

Andrea Arsiccio<sup>†</sup> and Joan-Emma Shea\*,<sup>†,‡</sup>

†Department of Chemistry and Biochemistry, University of California, Santa Barbara, California 93106, United States

‡Department of Physics, University of California, Santa Barbara, California 93106, United
States

E-mail: shea@ucsb.edu

#### Abstract

High pressures can be detrimental for protein stability, resulting in unfolding and loss of function. This phenomena occurs because the unfolding transition is accompanied by a decrease in volume, which is typically attributed to the elimination of cavities that are present within the native state as a result of packing defects. We present a novel computational approach that enables the study of pressure unfolding in atomistically detailed protein models in implicit solvent. We include the effect of pressure using a transfer free energy term that allows us to decouple the effect of protein residues and bound water molecules on the volume change upon unfolding. We discuss molecular dynamics simulations results using this protocol for two model proteins. Trp-cage and staphylococcal nuclease (SNase). We find that the volume reduction of bound water is the key energetic term that drives protein denaturation under the effect of pressure, for both Trp-cage and SNase. However, we note differences in unfolding mechanisms between the smaller Trp-cage and the larger SNase protein. Indeed, the unfolding of SNase, but not Trp-cage, is seen to be further accompanied by a reduction in the volume of internal cavities. Our results indicate that for small peptides, like Trp-cage, pressure denaturation is driven by the increase in solvent accessibility upon unfolding, and the subsequent increase in the number of bound water molecules. For larger proteins, like SNase, the cavities within the native fold act as weak spots, determining the overall resistance to pressure denaturation. Our simulations display a striking agreement with the pressure-unfolding profile experimentally obtained for SNase, and represent a promising approach for a computationally efficient and accurate exploration of pressure-induced denaturation of proteins.

## Introduction

Proteins are marginally stable molecules, whose structure can easily be disrupted, resulting in loss of their biological function. For instance, both high and low temperatures or extreme pH values may be detrimental for protein stability. The presence of surfaces, chemical denaturants or mechanical stress may further induce conformational changes with adverse effects on biological function.  $^{1-4}$ 

High pressures can also perturb the protein structure, <sup>5</sup> although this denaturation route is less investigated and the molecular mechanisms underlying pressure-induced unfolding of proteins remain controversial. <sup>6</sup> The following considerations hold for pressure-induced unfolding: if high pressure promotes the unfolding transition, this must mean that the volume of the system is reduced upon unfolding. The volume of a protein comprises the van der Waals volume of the protein atoms, void volumes due to packing defects of the native fold, <sup>7</sup> and the volume of the interacting water molecules. The van der Waals volume does not vary with the conformational state of the protein, and cannot therefore come into play in the volume reduction upon unfolding. The difference in void volumes between unfolded and native state is negative, although not all the voids in the native state contribute to the total volume change upon unfolding, <sup>8</sup> as some voids may still be present in the unfolded state ensemble. This void volume contribution certainly plays a major role in pressure denaturation, as changes in the amount of void volume within a protein were found to significantly modify the volume difference upon unfolding. <sup>9,10</sup>

In addition, the solvent accessible surface area (SASA) of proteins increases upon unfolding, and a larger number of water molecules will hence interact with the protein. If this interaction results in a change in density of the solvent molecules, this will also contribute to the effect of pressure on conformational stability. Water molecules may also penetrate the hydrophobic core, leading to the dissociation of hydrophobic contacts. <sup>11–13</sup> Furthermore, an additive approach developed by Chalikian et al., <sup>14</sup> in which the pressure-dependent differences in the apparent volume occupied by amino acids inside the protein core and when surface-exposed, has led to the hypothesis that solvation of the backbone atoms is a major driving force in pressure-induced denaturation.

In this paper, we build on the experimental results of Chalikian et al. <sup>14</sup> and implement an additive approach into an implicit solvent model in order to study pressure denaturation.

Implicit solvation models have the advantage of allowing faster equilibration times compared to their explicit counterpart. Indeed, the absence of the degrees of freedom corresponding to the solvent reduces the overall computational cost, and eliminates viscous friction effects, so that conformational transitions are accelerated. <sup>15</sup> We recently developed an implicit model that could account for temperature effects (including cold denaturation), <sup>16</sup> showing that many aspects of protein folding can still be captured without explicit solvent. To our knowledge, the only existing implicit solvent model that accounts for pressure effects is one that include a pressure-dependent perturbation term (the latter inspired by the works of Hillson et al. <sup>17</sup> and Hummer et al. <sup>12</sup>) coupled with the AWSEM coarse-grained model. <sup>18,19</sup>

Here we propose a novel method for the simulation of pressure effects in implicit solvent. This method is based on the use of free energies of transfer, and is compatible with an all-atom representation of the protein. The methodology is described in detail in the section "Theoretical Background", and allows us to separately describe the two main contributions involved in pressure unfolding, i.e., the volume change of the protein, and the volume change of bound water molecules. We test our approach on the  $\alpha$ -helical Trp-cage (NLYIQWLKDGGPSS-GRPPPS), and the globular protein staphylococcal nuclease (SNase). Trp-cage is a small peptide (20 residues) with known secondary structure and well-characterized free energy landscape, <sup>20</sup> that we used for our previous investigation in implicit solvent. <sup>16</sup> The pressure-induced unfolding of Trp-cage was also the subject of previous computational investigation in explicit solvent. <sup>21,22</sup> SNase was also included in our analysis because it is a well-known protein, whose folding behavior has been the subject of extensive experimental <sup>23–28</sup> and computational <sup>29–33</sup> investigation, including the study of pressure-induced unfolding. <sup>10,34–41</sup>

Our pressure-dependent potential shows an additive construction, making it possible to assess the energetic contributions involved in pressure unfolding and in this way gain new physical insights into the mechanisms underlying pressure denaturation. Exploiting this additivity, we find that the volume reduction of bound water seems to drive pressure-induced unfolding of both Trp-cage and SNase. For larger proteins, such as SNase, void

volumes present within the native structure disappear in the pressure-denatured state, as previously observed<sup>6,10</sup> acting as weak spots that facilitate the unfolding transition. For small peptides, like Trp-cage, the increase in solvent accessibility upon unfolding is key to explain the effect of pressure.

### Materials and Methods

#### Theoretical Background

The free energy of a peptide dissolved in water can be modelled as,

$$G^{tot} = E^{vac} + G^{el} + G^{np} \tag{1}$$

 $E^{vac}$  is the peptide energy in vacuum, sum of internal bonded contributions (bonds, angles, dihedrals) and non-bonded van der Waals interactions.  $G^{el}$  and  $G^{np}$  correspond to the polar and non-polar energies of hydration, respectively.

Eq. 1 is valid at ambient pressure  $P_0 = 1$  bar, and cannot be used to deal with the effects of pressure on protein behavior. Our aim is to add a further contribution  $G^{tr}(P)$  that depends on pressure P and that accounts for the pressure-induced denaturation of proteins. For this purpose, it is important to recall that the difference between the free energies of unfolding  $\Delta G$  at two different pressures  $P_0$  and P can be expressed as,

$$\Delta G(P) - \Delta G(P_0) = \int_{P_0}^{P} \Delta V(P) dP \tag{2}$$

where  $\Delta V(P)$  is the volume change upon unfolding, and is a function of pressure.

The volume change upon unfolding can be written as a Taylor expansion,

$$\Delta V(P) = \Delta V(P_0) - \Delta K(P_0)\Delta P - \frac{1}{2} \left( \frac{\partial \Delta K(P_0)}{\partial P} \right)_T \Delta P^2 + O(\Delta P^3)$$
 (3)

Here,  $\Delta K = -(\partial \Delta V/\partial P)_T$  is the change in compressibility upon unfolding and  $\Delta P = P - P_0$ .

Upon substitution of Eq. 3 into Eq. 2, the change in free energy of unfolding between P and  $P_0$  can be rewritten as,

$$\Delta G(P) - \Delta G(P_0) = \Delta V(P_0) \Delta P - \frac{1}{2} \Delta K(P_0) \Delta P^2 - \frac{1}{6} \left( \frac{\partial \Delta K(P_0)}{\partial P} \right)_T \Delta P^3 + O(\Delta P)^4$$
 (4)

#### Volume Change of the Protein

The volume change upon unfolding is linked to the elimination of a consistent fraction of the void volumes of the native state (i.e., those spaces inside the protein that are not occupied by atoms and that are not accessible to the solvent molecules), and to changes in the volume of hydration of the protein. Chalikian and Macgregor proposed an explanation of the molecular mechanisms underlying pressure-induced denaturation based on the pressure-dependent differences in the apparent volume occupied by amino acids when moved from the protein interior to the solvent. The authors made use of the average Voronoi volumes  $(V_{p,b})$  measured by Gerstein et al. 2-46 for the 20 naturally occurring amino acids, when deeply buried within the native protein core. Such Voronoi volumes include both the van der Waals volumes of each residue and the void around them. The presence of packing defects within the native fold of a protein is, therefore, implicitly taken into account in these Voronoi volumes, that are listed for the different side chains and for the backbone in the second column of Table S1.

Chalikian and Macgregor<sup>14</sup> also proposed values of apparent compressibility for the buried amino acid residues  $K_{p,b} = -(\partial V_{p,b}/\partial P)_T = V_{p,b}\beta_{p,b}$ , as well as for its derivative  $(\partial K_{p,b}/\partial P)_T = V_{p,b}[(\partial \beta_{p,b}/\partial P)_T - \beta_{p,b}^2]$ . These values were derived from experimental estimates of the average coefficient of isothermal compressibility of the interior of a native protein  $\beta_{p,b} = 25 \times 10^{-6} \text{ bar}^{-1}$  and of its pressure derivative  $(\partial \beta_{p,b}/\partial P)_T = -6.25 \times 10^{-9}$ 

bar<sup>-2</sup>. <sup>47–49</sup> Values of  $K_{p,b}$  and  $(\partial K_{p,b}/\partial P)_T$  are listed in the third and fourth column of Table S1, respectively.

The volumetric properties of solvent exposed side chains (volume  $V_{p,s}$  and apparent compressibility  $K_{p,s}$ ) were obtained from the partial molar volume and adiabatic compressibility data on N-acetyl amino acid amides. <sup>14,50</sup> The incremental change in the partial molar volume and adiabatic compressibility for oligoglycines with three and more peptide groups was instead used to determine the volumetric properties of the solvent-exposed backbone. <sup>51</sup> The pressure derivative  $(\partial K_{p,s}/\partial P)_T = 8.3 \times 10^{-7}$  cm<sup>3</sup> mol<sup>-1</sup> bar<sup>-2</sup> for the backbone is also experimentally available, <sup>52</sup> and was measured for Ala(Gly)<sub>n</sub> oligopeptides. Values of  $V_{p,s}$ ,  $K_{p,s}$  and  $(\partial K_{p,s}/\partial P)_T$  (when available) are listed in the fifth, sixth and seventh column of Table S1, respectively.

These volumetric data can be used to compute the change in free energy  $\Delta g_p^{sc}$  or  $^{bb}(P)$  upon exposure to the solvent of the backbone (superscript bb) or the amino acids side chains (superscript sc),

$$\Delta g_p^{sc \text{ or } bb}(P) = \Delta V_p^{sc \text{ or } bb}(P_0) \Delta P - \frac{1}{2} \Delta K_p^{sc \text{ or } bb}(P_0) \Delta P^2 - \frac{1}{6} \left( \frac{\partial \Delta K_p^{sc \text{ or } bb}(P_0)}{\partial P} \right)_T \Delta P^3 \quad (5)$$

where 
$$\Delta V_p^{sc \text{ or } bb} = V_{p,s}^{sc \text{ or } bb} - V_{p,b}^{sc \text{ or } bb}$$
 and  $\Delta K_p^{sc \text{ or } bb} = K_{p,s}^{sc \text{ or } bb} - K_{p,b}^{sc \text{ or } bb}$ .

Considering that the unfolding process involves exposure of residues from the native interior to the solvent, and assuming additivity, the following expression may hence be used to describe the change in free energy  $G_p^{tr}(P)$ , due to volumetric changes of the protein with pressure, in implicit solvent simulations,

$$G_p^{tr}(P) = \sum_{k=1}^n \Delta g_p^{sc,k}(P) \alpha^{sc,k} + \Delta g_p^{bb}(P) \sum_{k=1}^n \alpha^{bb,k}$$

$$\tag{6}$$

Here the summations runs over the total number n of amino acids in the protein, and  $\alpha^{sc,k}$  or bb,k is a fractional solvent accessibility, defined as the ratio between the solvent accession.

sible surface area (SASA) of each side chain or backbone, and the corresponding SASA in the tripeptide Gly - k - Gly,

$$\alpha^{sc,k \text{ or } bb,k} = \frac{SASA^{sc,k \text{ or } bb,k}}{SASA^{sc,k \text{ or } bb,k}_{Gly-k-Gly}} \tag{7}$$

The values of  $\Delta g_p^{sc,k}$  or bb(P) as function of pressure P are shown in Figure 1.

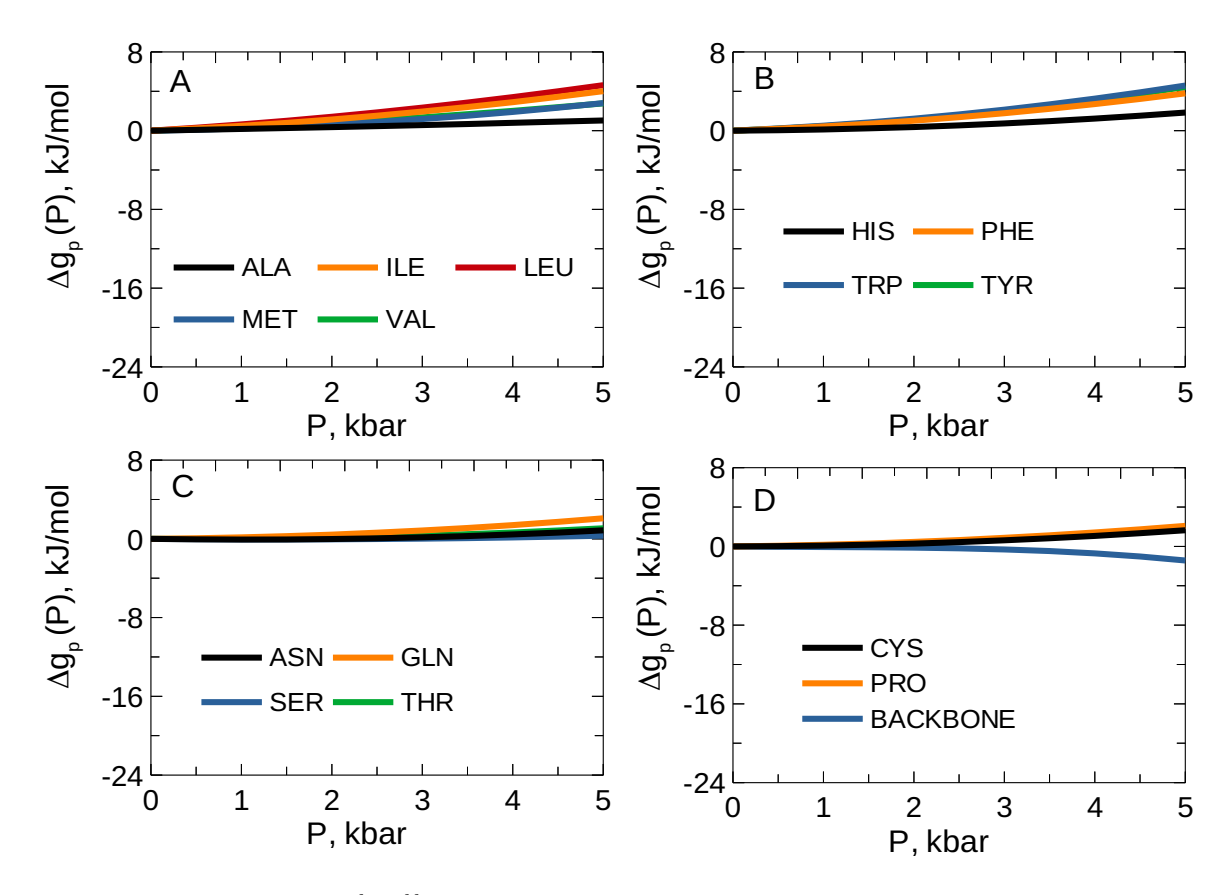


Figure 1: Values of  $\Delta g_p^{sc,k}$  or bb(P) as function of pressure P for the different side chains, and for the backbone.

It is important to note that the volumetric data of solvent-exposed side chains obtained from Chalikian and Macgregor<sup>14</sup> refer to uncharged forms of Asp, Glu, Lys and Arg. At neutral pH, these residues are charged, and electrostriction may probably reduce their volume, making the data for the uncharged form not completely reliable. For this reason, the side chains of Asp, Glu, Lys and Arg will not be considered in the first summation of Eq. 6, and the corresponding  $\Delta g_p^{sc,k}(P)$  values are not shown in Figure 1.

#### Volume Change of the Solvent

The term  $G_p^{tr}(P)$  includes only the contribution due to volume changes of the protein at a pressure  $P \neq P_0$ . However, the surrounding water molecules may also experience a volumetric change. For instance, Gerstein and Chothia  $^{53}$  found that water molecules near the protein surface have a mean volume  $V_{w,s} = 24.5 \text{ Å}^3$ , approximately 18% smaller than the volume of a molecule in bulk water  $(V_{w,b} = 29.7 \text{ Å}^3)$ . This means that if a protein unfolds and its SASA increases, then a larger number of water molecules will be close to the protein surface, and the overall volume of the system will experience a reduction. The volume reduction of the water molecules due to increased SASA of the protein and to pressure will have two effects: (1) a contribution  $G_{w,vp}^{tr}$  that promotes unfolding at higher pressures, because a system with reduced volume is energetically favored according to Eq. 4; (2) a contribution  $G_{w,ev}^{tr}$  that favors the native fold, due to the stabilizing excluded volume effect of a denser solvent, as predicted by scaled particle theory.  $^{54-58}$  These two opposing contributions should therefore be taken into account when computing the overall change  $G_w^{tr}(P)$  in the free energy of the system due to water,

$$G_w^{tr}(P) = G_{w,vp}^{tr}(P) + G_{w,ev}^{tr}(P)$$
 (8)

The  $G_{w,ev}^{tr}$  contribution is due to excluded-volume effects and can be computed as detailed in the Supporting Information file,

$$G_{w,ev}^{tr}(P) = RT \left[ \frac{r_w SASA}{V_{w,s}(P)} - \frac{r_w SASA}{V_{w,s}(P_0)} \right]$$
(9)

where  $r_w$  is the water molecules radius (1.4 Å), R is the universal gas constant, T is temperature and SASA is the total solvent accessible surface area of the protein.

The volume  $V_{w,s}(P_0)$  can be obtained from Gerstein and Chothia<sup>53</sup> ( $V_{w,s}(P_0) = 24.5 \text{ Å}^3$ ), while the value at pressure P can be calculated as,

$$V_{w,s}(P) = V_{w,s}(P_0) - V_{w,s}(P_0)\beta_{w,s}\Delta P$$
(10)

where  $\beta_{w,s}$  is the coefficient of isothermal compressibility of water in the first hydration shell of the protein. Persson and Halle<sup>59</sup> used molecular dynamics simulations to measure the coefficient of isothermal compressibility of water in the bulk ( $\beta_{w,b} = 0.504 \pm 0.011 \text{ GPa}^{-1}$ ), and in the first hydration shell of a protein ( $\beta_{w,s} = 0.348 \pm 0.007 \text{ GPa}^{-1}$ ). They found a difference between the two values, that will affect the volumetric behavior of water with pressure.

For a protein having n residues, and making use of the same additive construct employed in Eq. 6, Eq. 9 can eventually be rewritten as,

$$G_{w,ev}^{tr}(P) = RTr_w \left( \frac{1}{V_{w,s}(P)} - \frac{1}{V_{w,s}(P_0)} \right) \left( \sum_{k=1}^n SASA_{Gly-k-Gly}^{sc,k} \alpha^{sc,k} + \sum_{k=1}^n SASA_{Gly-k-Gly}^{bb,k} \alpha^{bb,k} \right)$$
(11)

The other contribution,  $\Delta G_{w,vp}^{tr}$ , is due to the reduction in the volume of water upon binding to the protein, and can be described by the following expression, similar to Eq. 6,

$$G_{w,vp}^{tr}(P) = \sum_{k=1}^{n} \Delta g_{w,vp}^{sc,k}(P) \alpha^{sc,k} + \sum_{k=1}^{n} \Delta g_{w,vp}^{bb,k}(P) \alpha^{bb,k}$$
(12)

where,

$$\Delta g_{w,vp}^{sc,k \text{ or } bb,k}(P) = \Delta V_w^{sc,k \text{ or } bb,k}(P_0)\Delta P - \frac{1}{2}\Delta K_w^{sc,k \text{ or } bb,k}(P_0)\Delta P^2$$

$$\tag{13}$$

 $\Delta V_w^{sc,k \text{ or } bb,k}$  and  $\Delta K_w^{sc,k \text{ or } bb,k}$  are computed as,

$$\Delta V_w^{sc,k \text{ or } bb,k} = \frac{2r_w SASA_{Gly-k-Gly}^{sc,k \text{ or } bb,k}}{V_{w,s}} (V_{w,s} - V_{w,b})$$
(14)

$$\Delta K_w^{sc,k \text{ or } bb,k} = \frac{2r_w SASA_{Gly-k-Gly}^{sc,k \text{ or } bb,k}}{V_{w,s}} (V_{w,s}\beta_{w,s} - V_{w,b}\beta_{w,b})$$
(15)

where the fraction  $(2r_wSASA_{Gly-k-Gly}^{sc,k})/V_{w,s}$  is used to count the number of water molecules in contact with residue k.

In summary, the solvent contribution may be expressed as,

$$G_w^{tr}(P) = \sum_{k=1}^{n} \Delta g_w^{sc,k}(P) \alpha^{sc,k} + \Delta g_w^{bb}(P) \sum_{k=1}^{n} \alpha^{bb,k}$$
 (16)

where,

$$\Delta g_w^{sc,k \text{ or } bb}(P) = RTr_w \left( \frac{1}{V_{w,s}(P)} - \frac{1}{V_{w,s}(P_0)} \right) SASA_{Gly-k-Gly}^{sc,k \text{ or } bb} + \Delta g_{w,vp}^{sc,k \text{ or } bb}(P)$$
 (17)

We note here that we are using in our modelling a residue-averaged decrease in the volume of water when moving from the bulk to the protein surface. We will show that this residue-averaged estimation of volume decrease upon binding to the protein seems to be sufficient in our simulations to reproduce the conformational changes induced by pressure, but future work could deepen this aspect even more, trying to introduce residue-specific values of differential solvent density.

In Eq. 17, a single value of  $SASA_{Gly-k-Gly}^{bb} = \sum_{k=1}^{20} SASA_{Gly-k-Gly}^{bb,k}/20 = 41.215 \text{ Å}^2$  has been introduced, by averaging over the 20 different amino acid types. This was done in order to obtain a single free energy of transfer contribution for the backbone group. The evolution of the  $\Delta g_w^{sc,k}$  or  $^{bb}(P)$  values with pressure is shown in Figure S1.

In the following, we will perform simulations at different temperatures and pressures. Therefore, Eq. 1 will be modified by the addition of two terms,

$$G^{tot} = E^{vac} + G^{el} + G^{np} + G^{tr}(P) + G^{tr}(T)$$
(18)

The first three terms describe a protein at  $T_0 = 298$  K and  $P_0 = 1$  bar. The  $G^{tr}(T)$  and  $G^{tr}(P)$  terms describe the transfer of the protein to a temperature  $T \neq T_0$  and pressure  $P \neq P_0$ , respectively.  $G^{tr}(T)$  will be modelled as described in approach 2 of our previous work, <sup>16</sup> where the temperature-dependent term  $G^{tr}(T)$  was obtained by mining a large set of PDB files obtained by nuclear magnetic resonance at different temperatures. Two different descriptions will instead be used for  $G^{tr}(P)$ ,

• Case 1 - protein contribution only:

$$G^{tr}(P) = G_p^{tr}(P) \tag{19}$$

In this case we will therefore neglect the contribution of the solvent, and consider only the volume changes of the protein.

• Case 2 - protein + water contributions:

$$G^{tr}(P) = G_p^{tr}(P) + G_w^{tr}(P) = G_p^{tr}(P) + G_{w,vp}^{tr}(P) + G_{w,ev}^{tr}(P)$$
(20)

In case 2, both the water and protein contributions will be considered. The evolution of the  $\Delta g_p^{sc,k}$  or  $^{bb}(P) + \Delta g_w^{sc,k}$  or  $^{bb}(P)$  values with pressure is shown in Figure 2 for the different side chains, and for the backbone.

We will imagine that the protein is first transferred from pressure  $P_0$  to pressure P at constant temperature  $T_0$ . For this reason, the temperature T in Eq. 11 will be set to  $T_0$ . This is consistent with the volumetric data used for  $G^{tr}(P)$ , that were evaluated at ambient temperature. Afterwards, the term  $G^{tr}(T)$  in Eq. 18 will move the protein, already at pressure P, from temperature  $T_0$  to temperature T. We will therefore make the implicit assumption that the term  $G^{tr}(T)$ , described in our previous work, <sup>16</sup> does not depend on pressure.

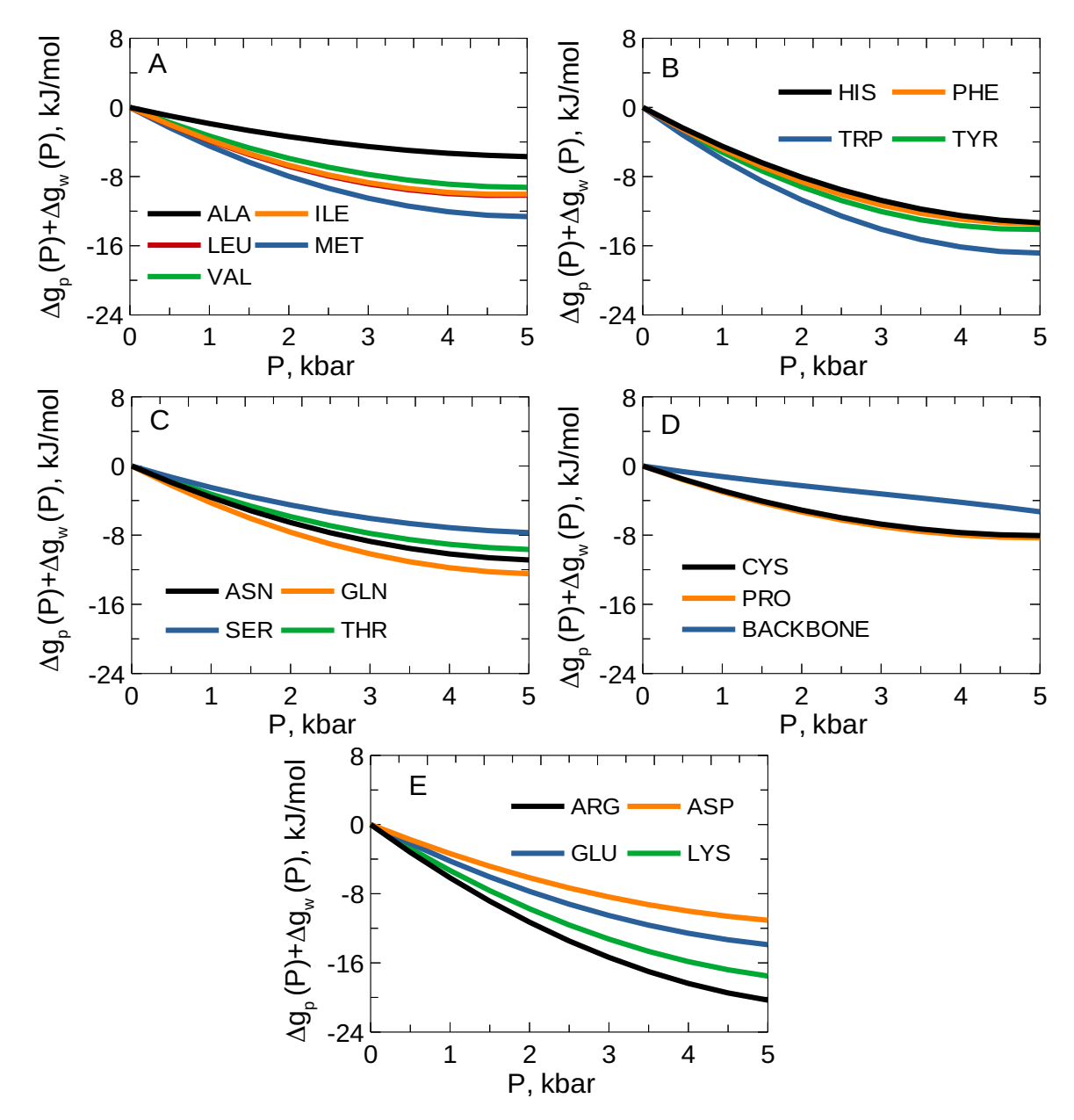


Figure 2: Values of  $\Delta g_p^{sc,k}$  or  $bb(P) + \Delta g_w^{sc,k}$  or bb(P) as function of pressure P for the different side chains, and for the backbone.

#### Simulation Details

Trp-cage (pdb 1L2Y<sup>60</sup>) at pH 7 and staphylococcal nuclease (SNase, pdb 1STN<sup>61</sup>) at pH 5.5 were used as model systems in our simulations. The protonation state of the proteins was adjusted using the H++ server, version 3.2 (http://biophysics.cs.vt.edu/H++<sup>62</sup>). We employed the Amber ff99SB-ILDB force field,  $^{63}$  and ran the trajectories on the AMBER 20 simulation suite,  $^{64}$  combined with Plumed 2.4.7.  $^{65}$  The generalized Born/surface area model of AMBER 20 was used to model the first three terms of Eq. 18. Specifically, we employed the OBC(II) model  $^{66}$  to estimate the Born radii (IGB = 5). The free energy of transfer terms  $G^{tr}(T)$  and  $G^{tr}(P)$  were added as external biases using Plumed, and we also took into account the effect of temperature and pressure on the dielectric constant. The equations proposed in Ref.  $^{67}$  were used for this purpose.

The systems were first energy minimized for 3000 steps using the steepest descent algorithm. Trp-cage was then simulated for 500 ns at different pressures in the range 1 bar-5 kbar, and at different temperatures in the range 270 K - 360 K. The first 200 ns were then discarded, and only the last 300 ns were used for the subsequent analyses. SNase was instead simulated for 250 ns at 298 K in the pressure range 1 kbar-3.5 kbar, and only the last 150 ns were used for analysis. Implicit solvent simulations significantly accelerate conformational transitions compared to their explicit counterpart, <sup>15</sup> and we checked that the collected trajectories for Trp-cage and SNase were fully converged (Figure S2). In all cases, temperature was controlled using Langevin dynamics, with a collision frequency of 1.0 ps<sup>-1</sup>. All bonds linking to hydrogen atoms were constrained using the SHAKE algorithm. <sup>68</sup> The center of mass translation and rotation were removed every 500 steps (1 ps), and no cut-off was used for the Coulombic and Lennard-Jones interactions. A time step of 2.0 fs was used and configurations were saved every 2 ps.

#### Analysis of the Trajectories

#### Secondary structure content

The  $\alpha$ -helix ( $\alpha$ ) and parallel (p $\beta$ ) or antiparallel (a $\beta$ )  $\beta$ -sheet content was computed as the number of residue sections having an  $\alpha$ -helical, parallel or antiparallel  $\beta$ -sheet configuration, <sup>69</sup>

$$\alpha/p\beta/a\beta = \sum_{\mu} g[r_{dist}(\{R_i\}_{i \in \Omega_{\mu}}, \{R^0\})]$$
(21)

Here the summation runs over all possible segments involved in the  $\alpha$ -helix or  $\beta$ -sheet.  $\{R_i\}_{i\in\Omega_\mu}$  are the atomic coordinates of a set  $\Omega_\mu$  of 6 residues of the protein, and  $g(r_{dist})$  is the following switching function,

$$g(r_{dist}) = \frac{1 - \left(\frac{r_{dist}}{r_0}\right)^8}{1 - \left(\frac{r_{dist}}{r_0}\right)^{12}}$$
(22)

 $r_{dist}$  is the distance RMSD with respect to a reference  $\alpha$ -helical, parallel or antiparallel  $\beta$ -sheet configuration  $\{R^0\}$ , and the cutoff distance  $r_0$  was set to 0.08 nm.

#### Cluster analysis

The conformations assumed by the proteins during the last 300 ns (Trp-cage) or 150 ns (SNase) of the simulation time were grouped together using the Daura algorithm. <sup>70</sup> A cutoff of 0.2 nm (Trp-cage) or 0.8 nm (SNase) on the root mean square deviations of the N-C $_{\alpha}$ -C atoms was used to cluster structures together. The most probable conformations were then visualized using the software VMD (Visual Molecular Dynamics). <sup>71</sup>

#### Hydrogen bond analysis

The number of within-peptide hydrogen bonds was also measured. A hydrogen bond was deemed to be present when the distance between donor and acceptor was less than 0.30 nm,

and the angle formed between the acceptor, hydrogen and donor atoms was greater than 135°.

#### Cavities/clefts analysis

The presence of cavities and clefts within the most probable conformations (isolated using the Daura algorithm<sup>70</sup>) was analyzed using the McVol algorithm<sup>72</sup> using a 1.1 Å probe sphere, as it was done already in previous work.<sup>10</sup>

## Results and Discussion

# The Volume Reduction of Bound Water is Necessary to Describe the Pressure Unfolding of Trp-cage and SNase

Chalikian and Macgregor<sup>14</sup> analyzed the volumetric properties of buried and exposed amino acids, obtaining graphs similar to those shown in Figure 1. It is evident that the volume change of amino acids is not dramatic when moving from the protein interior to the external solvent. In addition, the  $\Delta g_p^{sc,k}(P)$  contribution is positive, or close to zero, for most side chains. Only the backbone experiences a non negligible decrease in volume when exposed to the solvent, leading to a negative  $\Delta g_p(P)^{bb}$  (Figure 1D). Based on this observation, Chalikian and Macgregor concluded that the solvation of backbone atoms should play a major role in pressure-induced protein denaturation.

As a first objective, we therefore set out to investigate whether the negative  $\Delta g_p(P)^{bb}$  contribution alone could explain the pressure-induced unfolding of proteins. We ran implicit solvent simulations of Trp-cage at 5 kbar, and in the range 270 K-360 K, considering only the protein contribution to pressure-related effects (Eq. 19, case 1 in the Materials and Methods section). The results of this analysis are displayed in Figure 3 (red series). Similarly, SNase was simulated at 3.5 kbar and 298 K, considering only the protein contribution to pressure effects, and the results are shown in Figure 4 (red series). The protein radius of gyration  $R_q$ ,

 $\alpha$ -helix content for Trp-cage and folded fraction for SNase, end-to-end distance  $R_{ee}$ , backbone root mean square deviation (RMSD) compared to the crystal structure (pdb 1L2Y  $^{60}$  for Trp-cage and pdb 1STN  $^{61}$  for SNase), number of internal hydrogen bonds and solvent accessible surface area have been computed. In particular, the end-to-end distance  $R_{ee}$  was computed between the centers of mass of the first and last residues of the proteins, while the folded fraction of SNase was defined as the fraction of time during the equilibrated trajectory (last 150 ns) corresponding to a RMSD < 0.8 nm compared to the crystal structure. Errors were estimated by block averaging. Briefly, the equilibrated trajectories were divided into 4 blocks, and the standard deviation computed over the average values of the properties in each of the blocks.

When the protein contributions only were considered, no noticeable difference was observed between Trp-cage behavior at 1 bar (black curve in Figure 3) or 5 kbar (red curve). The radius of gyration (Figure 3A), end-to-end distance (Figure 3C), and solvent accessible surface area (Figure 3F) were almost superimposed. Some degree of stabilization at 5 kbar was even observed around 320 K, as in this case the  $\alpha$ -helix content (Figure 3B) was higher than at 1 bar, and the RMSD (Figure 3D) was slightly lower. These results indicate that the protein contribution only is not enough to explain pressure-induced unfolding of Trp-cage, as also emerges from the  $\alpha$ -helix content vs.  $R_g$  and  $R_{ee}$  vs.  $R_g$  distributions shown in Figure S3A,B.

Similarly, SNase simulated at 3.5 kbar does not unfold if the protein contribution only is considered. This is evident from the small radius of gyration (1.4573±0.0007 nm, red series in Figure 4A) obtained in this condition. The green curve in Figure 4A shows the evolution of SNase radius of gyration with pressure, as experimentally measured by Paliwal et al. <sup>34</sup> It was experimentally noted that SNase is stable until about 1500 bar, with a small radius of gyration of about 1.6 nm for the native basin. The pressure-unfolding transition occurs between 1500 and 3000 bar, and above 3500 bar SNase is completely unfolded, with a much larger radius of gyration of about 3.6 nm. When we consider only the protein contribution,

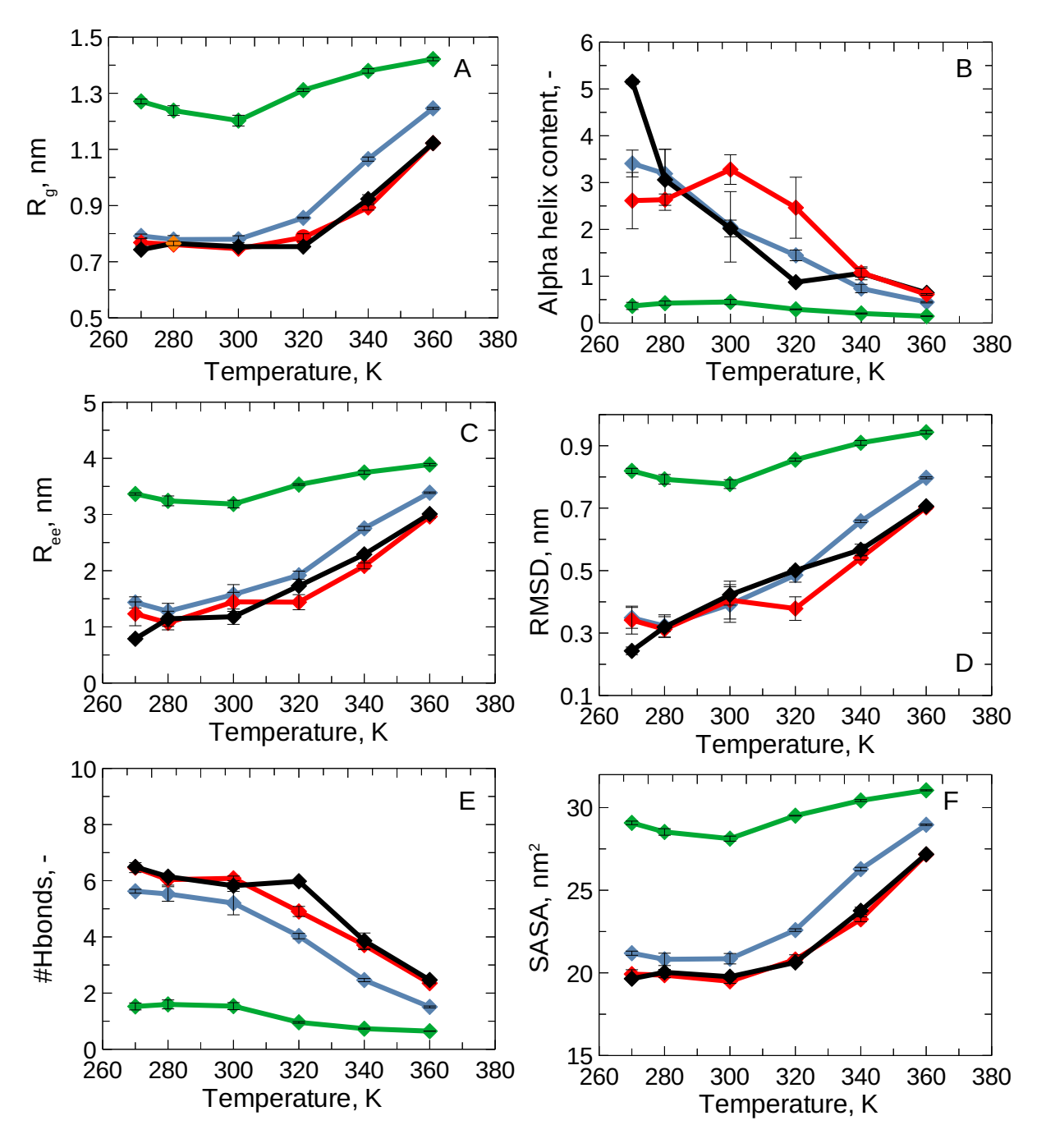


Figure 3: Evolution of (A) radius of gyration  $R_g$ , (B)  $\alpha$ -helix content, (C) end-to-end distance  $R_{ee}$ , (D) backbone RMSD compared to the crystal structure, (E) number of internal hydrogen-bonds, and (F) solvent accessible surface area of Trp-cage with temperature. Black line: 1 bar, red line: 5 kbar-protein contribution only (case 1), green line: 5 kbar-protein+water contributions (case 2), blue line: 1 kbar-protein+water contributions (case 2). Error bars show one standard deviation as calculated from block averaging.

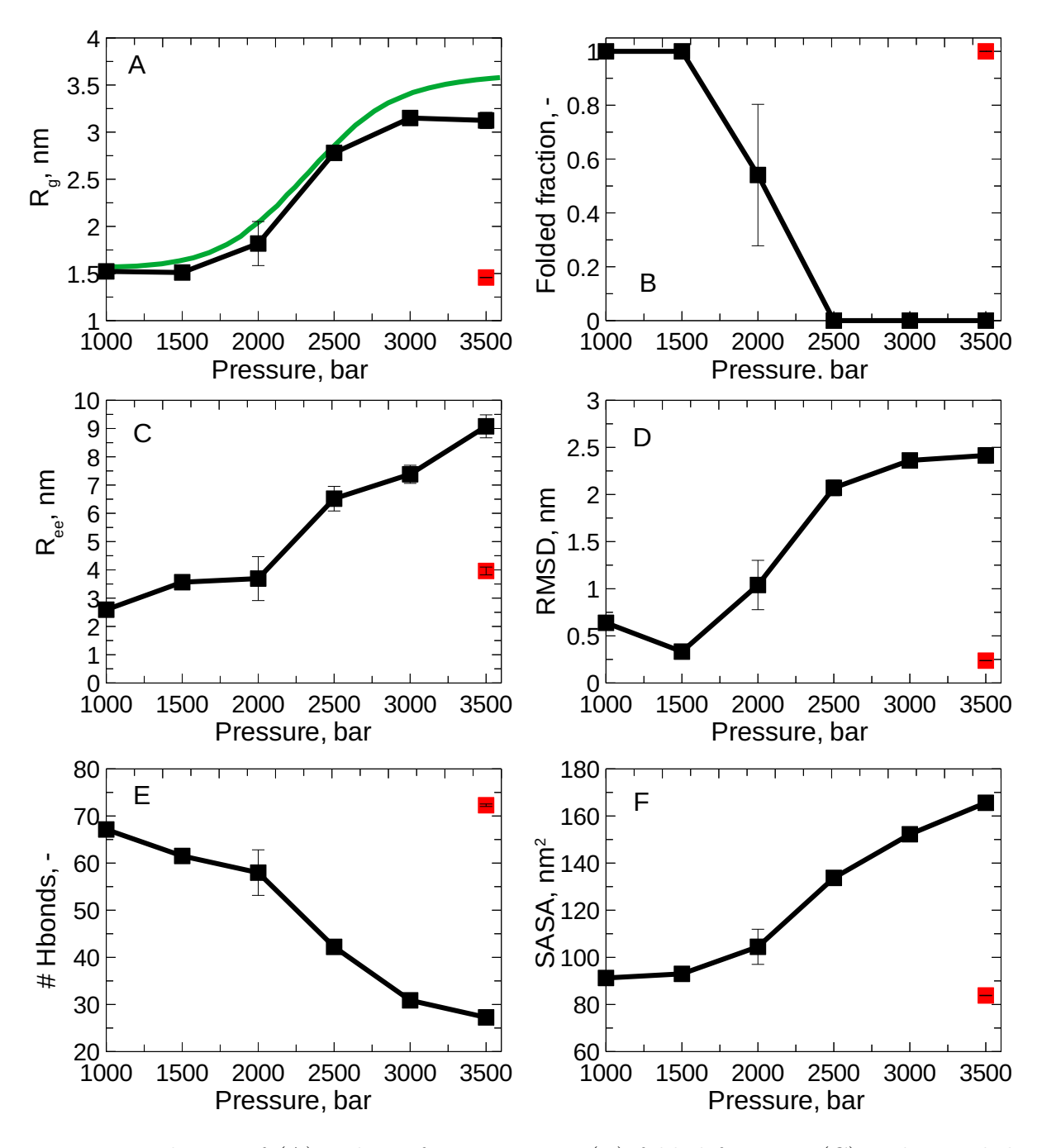


Figure 4: Evolution of (A) radius of gyration  $R_g$ , (B) folded fraction, (C) end-to-end distance  $R_{ee}$ , (D) backbone RMSD compared to the crystal structure, (E) number of internal hydrogen-bonds, and (F) solvent accessible surface area of SNase with pressure. Black line: protein+water contributions (case 2), red square: protein contribution only (case 1), green curve in panel A: experimental data from Paliwal et al. <sup>34</sup> Error bars show one standard deviation as calculated from block averaging.

the radius of gyration obtained from our simulations at 3500 bar clearly corresponds to the native basin. Also all the other indicators (folded fraction,  $R_{ee}$ , RMSD, number of hydrogen bonds, SASA) in the red series of Figure 4 are those of the native SNase, and the most sampled conformation in this condition shows a native-like secondary structure content (Figure S4A,B).

The negative (i.e., favourable to unfolding)  $\Delta g_p^{bb}(P)$  contribution for the backbone is therefore offset by the positive (i.e., unfavourable to unfolding)  $\Delta g_p^{sc,k}(P)$  contributions for the side chains. This translates into absence of destabilizing effect. The water term  $\Delta g_w^{sc,k} \circ bb(P)$  is, on the contrary, negative (i.e., favourable to unfolding) for all side chains and for the backbone (Figure S1). When added to the protein contribution, the total pressure term shown in Figure 2 is obtained. As can be seen, now also the side chains participate in unfolding.

When both the protein and the solvent contributions are considered, the pressure-induced unfolding of Trp-cage can be recovered (green and blue lines in Figure 3, obtained at 5 kbar or 1 kbar, respectively). At 1 kbar (blue line), the unfolding is not very pronounced around ambient temperature, and becomes remarkable only above 320 K (Figure S3C). This is evident from the evolution of the radius of gyration (Figure 3A) and RMSD (Figure 3D), where the blue and black curves are almost superimposed in the range 270-300 K. This result is in line with previous computational and experimental investigations of Trp-cage, <sup>21,73</sup> where high pressures were found to be needed for unfolding Trp-cage at low temperatures. However, adding a 1 kbar pressure reduces the number of internal hydrogen bonds (Figure 3E), and increases the solvent accessible surface area (Figure 3F) and end-to-end distance (Figure 3C) at any temperature.

If the pressure is further increased to 5 kbar (green line in Figure 3, and Figure S3D), complete unfolding of Trp-cage at any temperature is obtained. The protein structure in these conditions is very expanded (high radius of gyration and solvent accessibility), and shows negligible secondary structure content. The effect of temperature at 5 kbar is, on the

contrary, not very pronounced.

Also for SNase, addition of the water term (case 2, Eq. 20) succeeds in recovering the correct unfolding profile with pressure (Figures 4 and S5). The radius of gyration starts to increase above 2000 bar (black series in Figure 4A), showing a remarkable overlap with the experimental curve (in green). The folded fraction similarly decreases, eventually reaching a value of zero above 2500 bar (Figure 4B). Pressure-unfolding of SNase is accompanied by an increase in end-to-end distance (Figure 4C) and solvent accessible surface area (Figure 4F), and a disruption of the internal hydrogen bonding network (Figure 4E). The SNase structures obtained above 2500 bar display reduced secondary structure content, and a very expanded conformation (Figure S5).

The results herein illustrated indicate that the reduction of protein volume upon unfolding is not enough to explain the pressure-induced unfolding of Trp-cage and SNase. The solvent contribution needs also to be taken into account. When the protein unfolds, a larger number of water molecules will be in contact with the protein surface, and these molecules will have a smaller size, reducing the system volume.

# Pressure Unfolding is Driven by the Increase in Solvent Accessibility for Trp-cage, and the Elimination of Internal Cavities for SNase

We investigated the process of pressure unfolding further. We simulated Trp-cage at different pressures in the range 1-3500 bar, at either 280 or 300 K, including both the protein and solvent contributions (Figures 5 and S6).

We observed that the unfolding process of Trp-cage is gradual, with a noticeable effect on most secondary and tertiary structure indicators above 2000 bar at 300 K (black line in Figure 5) or 1500 bar at 280 K (red line). We previously observed that the solvent contribution is crucial for pressure unfolding, suggesting that the solvent accessible surface area exposed by the protein should play a crucial role. In line with this, the solvent accessibility of Trp-cage in Figure 5F displays a continuous and consistent increase with pressure.

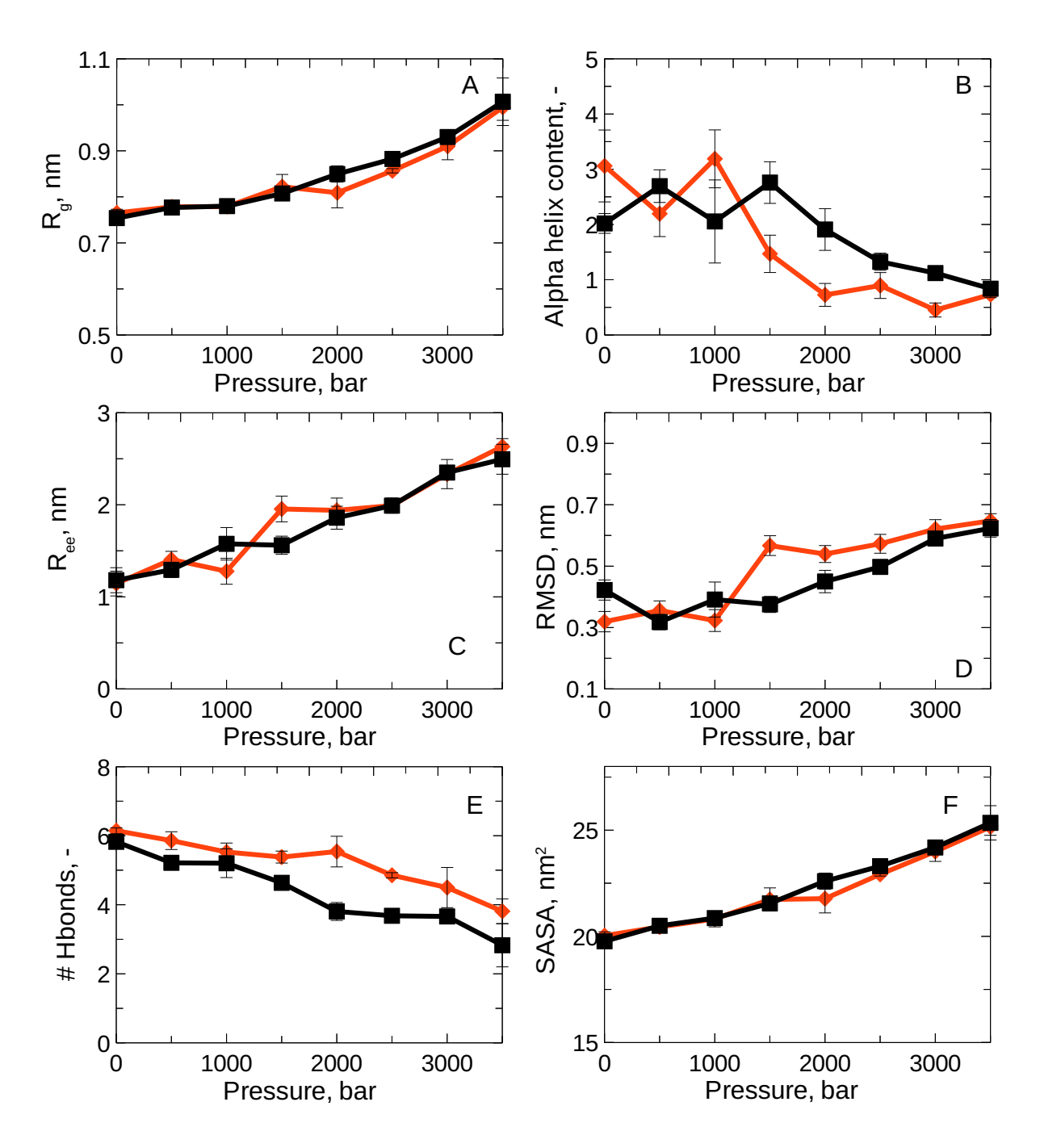


Figure 5: Evolution of (A) radius of gyration  $R_g$ , (B)  $\alpha$ -helix content, (C) end-to-end distance  $R_{ee}$ , (D) RMSD compared to the crystal structure, (E) number of internal hydrogen-bonds, and (F) solvent accessible surface area of Trp-cage with pressure. Black line: 300 K, red line: 280 K. Error bars show one standard deviation as calculated from block averaging.

We compared in greater detail Trp-cage conformations at the onset of hot (320 K and 1 bar, as identified in our previous work in which we developed an implicit solvent model that could account for temperature effects, <sup>16</sup> and as can be observed looking at the black line in Figure 3) and pressure (300 K and 2000 bar, black line in Figure 5) unfolding. We found (Figure 6) that Trp-cage displays a considerably larger solvent accessible surface area at 300 K and 2000 bar than at 320 K and 1 bar, suggesting once again that hydration effects are crucial for pressure denaturation.

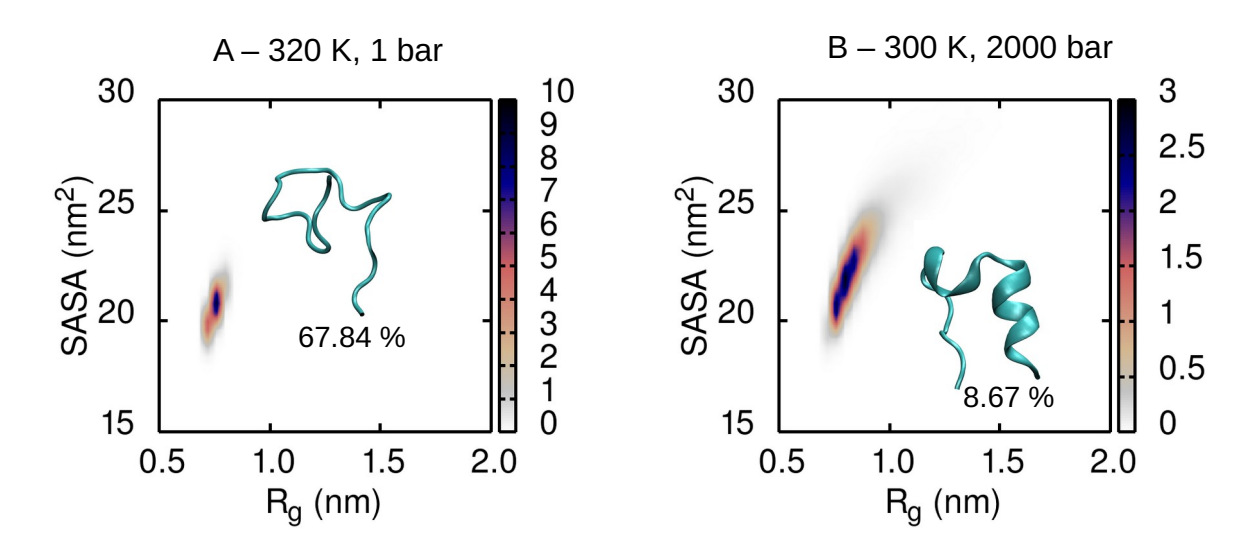


Figure 6: Distribution of Trp-cage SASA as function of the radius of gyration at the onet of hot (320 K, 1 bar) and pressure (300 K, 2000 bar) unfolding. The most probable conformation in each condition is also shown, with the corresponding probability.

Previous work suggested that the presence of void volumes inside the protein structure would play a major role in determining pressure unfolding, <sup>6,9,10,74,75</sup> while changes in the solvent density should be less important. Specifically, a good correlation was experimentally observed between the size of cavities within the native fold, and the sensitivity to pressure, while the change in SASA upon unfolding seemed to play a minor role.

These previous results from the literature are not in contrast with our simulations. Figure 7 shows the evolution of SNase cavities and clefts, as identified by the McVol program.<sup>72</sup> It is evident that, in line with previous results, internal void volumes within the native fold disappear during the unfolding process. It is also interesting and important to note

that at the onset of pressure unfolding (2 kbar), the C-terminal helix of SNase detaches from the rest of the protein, and the loop preceding this helix is partially disrupted. The structure we obtained from our simulations is extremely similar to an intermediate observed experimentally under pressure.<sup>10</sup>

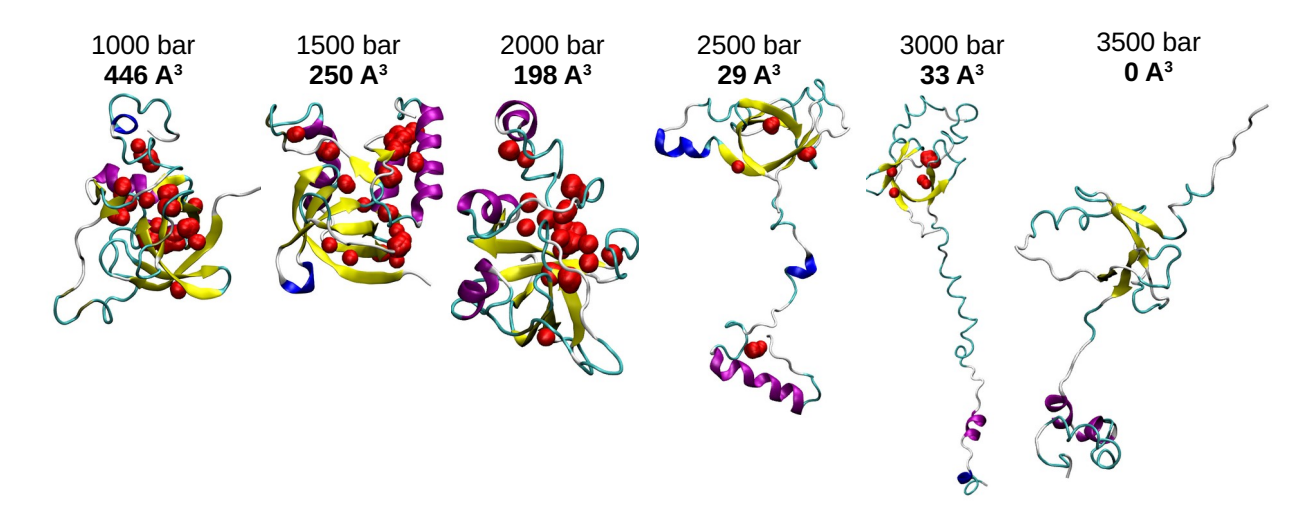


Figure 7: Volume of SNase cavities and clefts, as identified by the McVol program. <sup>72</sup> Cavities are shown as red beads in the cartoon representations of SNase structures.

Cavities are therefore crucial for the pressure denaturation of SNase also in our simulations, as experimentally observed. <sup>10</sup> However, this does not necessarily mean, as it was previously inferred, that the role of hydration is marginal. This can be better explained using the following analogy. We can imagine a vessel under the effect of internal pressure, and equipped with some weak areas, that act as vents. If pressure increases, the weak areas will be the first to break, because of their lower resistance. In addition, the larger the surface of these weak areas, the smaller the pressure endured by the vessel. However, the actual mechanism underlying the explosion is the pressure build-up inside the vessel and the possibility for this pressure to be released in a larger environment upon breakage of the weak areas. Cavities within the native fold of a protein act as vents, i.e., they are weak spots that determine the overall resistance to pressure denaturation. However, disruption of these cavities translates into an increased SASA, and the actual mechanism behind unfolding is the reduction in solvent volume that accompanies this process. Only when the solvent contribu-

tion is taken into account, can the unfolding profile of SNase be recovered in our simulations, displaying a striking agreement with the evolution of  $R_g$  experimentally measured (Figure 4A). If the protein contribution only is considered, cavities and clefts in SNase are stable even at 3500 bar (Figure S4C). Our proposed mechanism for pressure-induced unfolding is also in line with the previous hypothesis that water molecules may penetrate the hydrophobic core during pressure denaturation, disrupting the hydrophobic contacts. <sup>11–13</sup>

The case of Trp-cage is different, as the protein size and internal hydrophobic core are too small to account for an important role of cavities and clefts. As already observed in previous work, <sup>10</sup> the contribution from hydration density is thereby expected to be even more apparent in model systems such as Trp-cage, as confirmed by our results.

## Conclusions

In this paper we have addressed the problem of protein unfolding induced by pressure. Two model proteins, Trp-cage and SNase, have been selected for this investigation. We have developed an implicit solvent approach, based on the concept of free energies of transfer, to describe the effect of pressure. Our modelling approach considers two energetic contributions, i.e., the volume change of the protein, and the volume change of bound water molecules.

We have performed simulations with the objective to dissect these two contributions, and thus evaluate their relative importance in determining pressure unfolding. Interestingly, we have found that the volume change of the protein is not enough to explain the effect of pressure, and the water contribution has to be taken into account to recover the unfolding transition. Our results support the hypothesis that hydration effects are crucial to describe the pressure-induced unfolding of proteins.

For small systems, like Trp-cage, denaturation is accompanied by a consistent increase in solvent accessibility. A larger number of water molecules can interact with the extended conformation of the protein, reducing the overall volume of the system and as such promoting the unfolding transition. For larger proteins, like SNase, pressure denaturation is accompanied by the concomitant elimination of cavities present within the native fold and due to packing defects. These void volumes act as weak spots, being filled by water during unfolding and determining the overall resistance to pressure.

The implicit solvent approach proposed in the present work allows an efficient sampling of conformational space, and shows an excellent agreement with the pressure-unfolding profile obtained experimentally for SNase. Our approach provides a valid alternative to explicit solvent simulations, whose convergence at high pressure is problematic because of the slow conformational changes observed in these conditions.

## **Supporting Information**

Volumetric parameters, excluded volume contribution  $G_{w,ev}^{tr}(P)$  of water to pressure-induced unfolding, values of  $\Delta g_w^{sc,k}$  or  $^{bb}(P)$  as function of pressure, convergence graphs, distribution of  $\alpha$ -helix content and end-to-end distance as function of the radius of gyration for Trp-cage, distribution of the  $\alpha$ -helix and  $\beta$ -sheet content as function of the radius of gyration for SNase, most sampled conformations of Trp-cage and SNase during the simulations.

## Acknowledgement

The authors acknowledge support from the Center for Scientific Computing at the California Nanosystems Institute (CNSI, NSF grant CNS-1725797) for the availability of high performance computing resources and support. This work used the Extreme Science and Engineering Discovery Environment, which is supported by the National Science Foundation grant number ACI-1548562 (MCA05S027). The authors aknowledge support from the NSF (MCB-1716956) and the NIH (R01-GM118560-01A).

## References

- (1) Goldenzweig, A.; Fleishman, S. J. Principles of Protein Stability and Their Application in Computational Design. *Annu. Rev. Biochem.* **2018**, *87*, 105–129.
- (2) Arsiccio, A.; McCarty, J.; Pisano, R.; Shea, J.-E. Effect of Surfactants on Surface-Induced Denaturation of Proteins: Evidence of an Orientation-Dependent Mechanism. J. Phys. Chem. B 2018, 122, 11390–11399.
- (3) Bennion, B. J.; Daggett, V. The molecular basis for the chemical denaturation of proteins by urea. *Proc. Natl. Acad. Sci.* **2003**, *100*, 5142–5147.
- (4) Camilloni, C.; Guerini Rocco, A.; Eberini, I.; Gianazza, E.; Broglia, R.; Tiana, G. Urea and Guanidinium Chloride Denature Protein L in Different Ways in Molecular Dynamics Simulations. *Biophys. J.* 2008, 94, 4654–4661.
- (5) Bridgman, P. The Coagulation of Albumin by Pressure. J. Biol. Chem. 1914, 19, 511–512.
- (6) Roche, J.; Royer, C. A. Lessons from pressure denaturation of proteins. J. R. Soc. Interface 2018, 15, 20180244.
- (7) Rashin, A. A.; Iofin, M.; Honig, B. Internal cavities and buried waters in globular proteins. *Biochemistry* **1986**, *25*, 3619–3625.
- (8) Chen, C. R.; Makhatadze, G. I. Molecular determinant of the effects of hydrostatic pressure on protein folding stability. *Nat. Commun.* **2017**, *8*, 14561.
- (9) Ando, N.; Barstow, B.; Baase, W. A.; Fields, A.; Matthews, B. W.; Gruner, S. M. Structural and Thermodynamic Characterization of T4 Lysozyme Mutants and the Contribution of Internal Cavities to Pressure Denaturation. *Biochemistry* 2008, 47, 11097–11109.

- (10) Roche, J.; Caro, J. A.; Norberto, D. R.; Barthe, P.; Roumestand, C.; Schlessman, J. L.; Garcia, A. E.; García-Moreno E., B.; Royer, C. A. Cavities determine the pressure unfolding of proteins. *Proc. Natl. Acad. Sci.* 2012, 109, 6945–6950.
- (11) Ghosh, T.; García, A. E.; Garde, S. Molecular Dynamics Simulations of Pressure Effects on Hydrophobic Interactions. *J. Am. Chem. Soc.* **2001**, *123*, 10997–11003.
- (12) Hummer, G.; Garde, S.; García, A. E.; Paulaitis, M. E.; Pratt, L. R. The pressure dependence of hydrophobic interactions is consistent with the observed pressure denaturation of proteins. *Proc. Natl. Acad. Sci.* **1998**, *95*, 1552–1555.
- (13) Collins, M. D.; Hummer, G.; Quillin, M. L.; Matthews, B. W.; Gruner, S. M. Cooperative water filling of a nonpolar protein cavity observed by high-pressure crystallography and simulation. *Proc. Natl. Acad. Sci.* **2005**, *102*, 16668–16671.
- (14) Chalikian, T. V.; Macgregor, R. B. Origins of Pressure-Induced Protein Transitions. J. Mol. Biol. 2009, 394, 834 – 842.
- (15) Anandakrishnan, R.; Drozdetski, A.; Walker, R. C.; Onufriev, A. V. Speed of Conformational Change: Comparing Explicit and Implicit Solvent Molecular Dynamics Simulations. *Biophys. J.* 2015, 108, 1153–1164.
- (16) Arsiccio, A.; Shea, J.-E. Protein Cold Denaturation in Implicit Solvent Simulations: A Transfer Free Energy Approach. J. Phys. Chem. B 2021, 125, 5222–5232.
- (17) Hillson, N.; Onuchic, J. N.; García, A. E. Pressure-induced protein-folding/unfolding kinetics. Proc. Natl. Acad. Sci. 1999, 96, 14848–14853.
- (18) Davtyan, A.; Schafer, N. P.; Zheng, W.; Clementi, C.; Wolynes, P. G.; Papoian, G. A. AWSEM-MD: Protein Structure Prediction Using Coarse-Grained Physical Potentials and Bioinformatically Based Local Structure Biasing. J. Phys. Chem. B 2012, 116, 8494–8503.

- (19) Sirovetz, B. J.; Schafer, N. P.; Wolynes, P. G. Water Mediated Interactions and the Protein Folding Phase Diagram in the Temperature–Pressure Plane. J. Phys. Chem. B 2015, 119, 11416–11427.
- (20) Streicher, W. W.; Makhatadze, G. I. Unfolding Thermodynamics of Trp-Cage, a 20 Residue Miniprotein, Studied by Differential Scanning Calorimetry and Circular Dichroism Spectroscopy. *Biochemistry* 2007, 46, 2876–2880.
- (21) Day, R.; Paschek, D.; Garcia, A. E. Microsecond simulations of the folding/unfolding thermodynamics of the Trp-cage miniprotein. *Proteins* **2010**, *78*, 1889–1899.
- (22) Paschek, D.; Hempel, S.; García, A. E. Computing the stability diagram of the Trp-cage miniprotein. *Proc. Natl. Acad. Sci.* **2008**, *105*, 17754–17759.
- (23) Shortle, D. Guanidine hydrochloride denaturation studies of mutant forms of staphylococcal nuclease. J. Cell. Biochem. 1986, 30, 281–289.
- (24) Shortle, D. In *Protein Stability*; Anfinsen, C., Richards, F. M., Edsall, J. T., Eisenberg, D. S., Eds.; Adv. Protein Chem.; Academic Press: Cambridge, MA, USA, 1995; Vol. 46; pp 217–247.
- (25) Ionescu, R. M.; Eftink, M. R. Global Analysis of the Acid-Induced and Urea-Induced Unfolding of Staphylococcal Nuclease and Two of Its Variants. *Biochemistry* 1997, 36, 1129–1140.
- (26) Carra, J. H.; Privalov, P. L. Energetics of Denaturation and m Values of Staphylococcal Nuclease Mutants. *Biochemistry* **1995**, *34*, 2034–2041.
- (27) Griko, Y. V.; Privalov, P. L.; Sturtevant, J. M.; SYu, V. Cold denaturation of staphylococcal nuclease. *Proc. Natl. Acad. Sci.* **1988**, *85*, 3343–3347.

- (28) Kataoka, M. In *Molecular Science of Fluctuations Toward Biological Functions*; Terazima, M., Kataoka, M., Ueoka, R., Okamoto, Y., Eds.; Springer Japan: Tokyo, 2016; pp 151–161.
- (29) Smolin, N.; Winter, R. Molecular Dynamics Simulations of Staphylococcal Nuclease: Properties of Water at the Protein Surface. J. Phys. Chem. B **2004**, 108, 15928–15937.
- (30) Chatfield, D. C.; Szabo, A.; Brooks, B. R. Molecular Dynamics of Staphylococcal Nuclease: Comparison of Simulation with 15N and 13C NMR Relaxation Data. J. Am. Chem. Soc. 1998, 120, 5301–5311.
- (31) Yamaotsu, N.; Moriguchi, I.; Kollman, P. A.; Hirono, S. Molecular dynamics study of the stability of staphylococcal nuclease mutants: component analysis of the free energy difference of denaturation. *Biochim. Biophys. Acta* **1993**, *1163*, 81–88.
- (32) Damjanović, A.; García-Moreno, B.; Lattman, E. E.; García, A. E. Molecular dynamics study of water penetration in staphylococcal nuclease. *Proteins* **2005**, *60*, 433–449.
- (33) Pathak, A. K. Constant pH molecular dynamics study on the doubly mutated staphylococcal nuclease: capturing the microenvironment. RSC Adv. 2015, 5, 94926–94932.
- (34) Paliwal, A.; Asthagiri, D.; Bossev, D. P.; Paulaitis, M. E. Pressure Denaturation of Staphylococcal Nuclease Studied by Neutron Small-Angle Scattering and Molecular Simulation. *Biophys. J.* 2004, 87, 3479–3492.
- (35) Woenckhaus, J.; Köhling, R.; Thiyagarajan, P.; Littrell, K. C.; Seifert, S.; Royer, C. A.; Winter, R. Pressure-Jump Small-Angle X-Ray Scattering Detected Kinetics of Staphylococcal Nuclease Folding. *Biophys. J.* **2001**, *80*, 1518–1523.
- (36) Lassalle, M. W.; Yamada, H.; Akasaka, K. The pressure-temperature free energy-landscape of staphylococcal nuclease monitored by <sup>1</sup>H NMR. *J. Mol. Biol.* **2000**, *298*, 293–302.

- (37) Panick, G.; Malessa, R.; Winter, R.; Rapp, G.; Frye, K. J.; Royer, C. A. Structural characterization of the pressure-denatured state and unfolding/refolding kinetics of staphylococcal nuclease by synchrotron small-angle X-ray scattering and Fourier-transform infrared spectroscopy. J. Mol. Biol. 1998, 275, 389–402.
- (38) Panick, G.; Vidugiris, G. J. A.; Malessa, R.; Rapp, G.; Winter, R.; Royer, C. A. Exploring the Temperature-Pressure Phase Diagram of Staphylococcal Nuclease. *Biochemistry* 1999, 38, 4157–4164.
- (39) Frye, K. J.; Perman, C. S.; Royer, C. A. Testing the Correlation between ΔA and ΔV of Protein Unfolding Using m Value Mutants of Staphylococcal Nuclease. *Biochemistry* 1996, 35, 10234–10239.
- (40) Frye, K. J.; Royer, C. A. Probing the contribution of internal cavities to the volume change of protein unfolding under pressure. *Protein Sci.* **1998**, *7*, 2217–2222.
- (41) Mitra, L.; Hata, K.; Kono, R.; Maeno, A.; Isom, D.; Rouget, J.-B.; Winter, R.; Akasaka, K.; García-Moreno, B.; Royer, C. A. Vi-Value Analysis: A Pressure-Based Method for Mapping the Folding Transition State Ensemble of Proteins. J. Am. Chem. Soc. 2007, 129, 14108–14109.
- (42) Gerstein, M.; Sonnhammer, E. L.; Chothia, C. Volume changes in protein evolution. *J. Mol. Biol.* **1994**, *236*, 1067 1078.
- (43) Gerstein, M.; Tsai, J.; Levitt, M. The Volume of Atoms on the Protein Surface: Calculated from Simulation, using Voronoi Polyhedra. J. Mol. Biol. 1995, 249, 955 966.
- (44) Tsai, J.; Taylor, R.; Chothia, C.; Gerstein, M. The packing density in proteins: standard radii and volumes11Edited by J. M. Thornton. J. Mol. Biol. 1999, 290, 253 266.
- (45) Tsai, J.; Gerstein, M. Calculations of protein volumes: sensitivity analysis and parameter database. *Bioinformatics* **2002**, *18*, 985–995.

- (46) Harpaz, Y.; Gerstein, M.; Chothia, C. Volume changes on protein folding. *Structure* 1994, 2, 641–649.
- (47) Taulier, N.; Chalikian, T. V. Compressibility of protein transitions. *Biochim. Biophys.*Acta 2002, 1595, 48 70.
- (48) Kharakoz, D. P. Protein Compressibility, Dynamics, and Pressure. *Biophys. J.* **2000**, 79, 511 525.
- (49) Chalikian, T. V. Volumetric Properties of Proteins. Annu. Rev. Biophys. Biomol. Struct. 2003, 32, 207–235.
- (50) Lee, S.; Tikhomirova, A.; Shalvardjian, N.; Chalikian, T. V. Partial molar volumes and adiabatic compressibilities of unfolded protein states. *Biophys. Chem.* 2008, 134, 185 199.
- (51) Chalikian, T. V.; Sarvazyan, A. P.; Funck, T.; Breslauer, K. J. Partial molar volumes, expansibilities, and compressibilities of oligoglycines in aqueous solutions at 18–55°C. *Biopolymers* **1994**, *34*, 541–553.
- (52) Hedwig, G. R.; Høgseth, E.; Høiland, H. Volumetric properties of the glycyl group of proteins in aqueous solution at high pressures. *Phys. Chem. Chem. Phys.* **2008**, *10*.
- (53) Gerstein, M.; Chothia, C. Packing at the protein-water interface. *Proc. Natl. Acad. Sci.* **1996**, *93*, 10167–10172.
- (54) Reiss, H.; Frisch, H. L.; Lebowitz, J. L. Statistical Mechanics of Rigid Spheres. *J. Chem. Phys.* **1959**, *31*, 369–380.
- (55) Tang, K. E.; Bloomfield, V. A. Excluded Volume in Solvation: Sensitivity of Scaled-Particle Theory to Solvent Size and Density. *Biophys. J.* **2000**, *79*, 2222 2234.
- (56) Lebowitz, J. L.; Helfand, E.; Praestgaard, E. Scaled Particle Theory of Fluid Mixtures.

  J. Chem. Phys. 1965, 43, 774–779.

- (57) Mandell, M. J.; Reiss, H. Scaled particle theory: Solution to the complete set of scaled particle theory conditions: Applications to surface structure and dilute mixtures. *J. Stat. Phys.* **1975**, *13*, 113–128.
- (58) Heying, M.; Corti, D. S. Scaled Particle Theory Revisited: New Conditions and Improved Predictions of the Properties of the Hard Sphere Fluid. J. Phys. Chem. B 2004, 108, 19756–19768.
- (59) Persson, F.; Halle, B. Compressibility of the protein-water interface. *J. Chem. Phys.* **2018**, *148*, 215102.
- (60) Neidigh, J. W.; Fesinmeyer, R. M.; Andersen, N. H. Designing a 20-residue protein.

  Nat. Struct. Biol. 2002, 9, 425–430.
- (61) Hynes, T. R.; Fox, R. O. The crystal structure of staphylococcal nuclease refined at 1.7 Å resolution. *Proteins* **1991**, *10*, 92–105.
- (62) Anandakrishnan, R.; Aguilar, B.; Onufriev, A. V. H++ 3.0: Automating pK prediction and the preparation of biomolecular structures for atomistic molecular modeling and simulations. *Nucleic Acids Res.* **2012**, 40, W537–W541.
- (63) Lindorff-Larsen, K.; Piana, S.; Palmo, K.; Maragakis, P.; Klepeis, J. L.; Dror, R. O.; Shaw, D. E. Improved side-chain torsion potentials for the Amber ff99SB protein force field. *Proteins* 2010, 78, 1950–1958.
- (64) Pearlman, D. A.; Case, D. A.; Caldwell, J. W.; Ross, W. S.; Cheatham, T. E.; De-Bolt, S.; Ferguson, D.; Seibel, G.; Kollman, P. AMBER, a package of computer programs for applying molecular mechanics, normal mode analysis, molecular dynamics and free energy calculations to simulate the structural and energetic properties of molecules. Comput. Phys. Commun. 1995, 91, 1 41.

- (65) Tribello, G. A.; Bonomi, M.; Branduardi, D.; Camilloni, C.; Bussi, G. PLUMED 2: New feathers for an old bird. *Comput. Phys. Commun.* **2014**, *185*, 604 613.
- (66) Onufriev, A.; Bashford, D.; Case, D. A. Exploring protein native states and large-scale conformational changes with a modified generalized born model. *Proteins* **2004**, *55*, 383–394.
- (67) Bradley, D. J.; Pitzer, K. S. Thermodynamics of electrolytes. 12. Dielectric properties of water and Debye-Hueckel parameters to 350.degree.C and 1 kbar. J. Phys. Chem. 1979, 83, 1599–1603.
- (68) Ryckaert, J.-P.; Ciccotti, G.; Berendsen, H. J. Numerical integration of the cartesian equations of motion of a system with constraints: molecular dynamics of n-alkanes. *J. Comput. Phys.* **1977**, *23*, 327 341.
- (69) Pietrucci, F.; Laio, A. A Collective Variable for the Efficient Exploration of Protein Beta-Sheet Structures: Application to SH3 and GB1. J. Chem. Theory . Comput. 2009, 5, 2197–2201.
- (70) Daura, X.; Gademann, K.; Jaun, B.; Seebach, D.; van Gunsteren, W. F.; Mark, A. E. Peptide Folding: When Simulation Meets Experiment. Angew. Chem. Int. Ed. 1999, 38, 236–240.
- (71) Humphrey, W.; Dalke, A.; Schulten, K. VMD: Visual molecular dynamics. J. Mol. Graph. 1996, 14, 33 38.
- (72) Till, M. S.; Ullmann, G. M. McVol A program for calculating protein volumes and identifying cavities by a Monte Carlo algorithm. *J. Mol. Model.* **2010**, *16*, 419–429.
- (73) Kitazawa, S.; Fossat, M. J.; McCallum, S. A.; Garcia, A. E.; Royer, C. A. NMR and Computation Reveal a Pressure-Sensitive Folded Conformation of Trp-Cage. J. Phys. Chem. B 2017, 121, 1258–1267.

- (74) Rouget, J.-B.; Aksel, T.; Roche, J.; Saldana, J.-L.; Garcia, A. E.; Barrick, D.; Royer, C. A. Size and Sequence and the Volume Change of Protein Folding. J. Am. Chem. Soc. 2011, 133, 6020–6027.
- (75) Rouget, J.-B.; Schroer, M. A.; Jeworrek, C.; Puhse, M.; Saldana, J.-L.; Bessin, Y.; Tolan, M.; Barrick, D.; Winter, R.; Royer, C. A. Unique Features of the Folding Landscape of a Repeat Protein Revealed by Pressure Perturbation. *Biophys. J.* **2010**, *98*, 2712–2721.

# **Graphical TOC Entry**

